Title
Axial and radial thermal responses of energy pile under six storey residential building

Journal
Canadian Geotechnical Journal, 56(7)

ISSN
0008-3674

Authors
Faizal, Mohammed
Bouazza, Abdelmalek
McCartney, John S
et al.

Publication Date
2019-07-01

DOI
10.1139/cgj-2018-0246

Peer reviewed

Canadian Science Publishing | Canadian Geotechnical Journal

Axial and radial thermal responses of an energy pile under a 6-storey residential building

Journal:	*Canadian Geotechnical Journal*
Manuscript ID	cgj-2018-0246.R1
Manuscript Type:	Article
Date Submitted by the Author:	12-Sep-2018
Complete List of Authors:	Faizal, Mohammed; Monash University Bouazza, Abdelmalek; Monash University, McCartney, John; University of California San Diego, Structural Engineering Haberfield, Chris; Golder Associates Pty Ltd,
Keyword:	Energy Piles, Field tests, Thermal response, Stress/strains
Is the invited manuscript for consideration in a Special Issue? :	Not applicable (regular submission)

Axial and radial thermal responses of an energy pile under a 6-storey residential building

by

Mohammed Faizal

PhD Student, Monash University, Department of Civil Engineering, 23 College Walk, Clayton, Vic. 3800, Australia. Telephone: +61 3 9905 8901; Email: mohammed.faizal@monash.edu

*** Abdelmalek Bouazza (Corresponding Author)**

Professor, Monash University, Department of Civil Engineering, 23 College Walk, Clayton, Vic. 3800, Australia. Telephone: +61 3 9905 4956; Email: malek.bouazza@monash.edu

John S. McCartney

Professor, University of California San Diego, Department of Structural Engineering, 9500 Gilman Drive, SME 442J, La Jolla, CA 92093-0085, USA, Telephone: +1 858 534 9630; Email: mccartney@ucsd.edu

Chris Haberfield

Principal, Golder Associates Pty. Ltd., Building 7, Botanicca Corporate Park, 570–588 Swan St., Richmond, Vic. 3121, Australia. Telephone: +61 3 8862 3586; Email: chaberfield@golder.com.au

Abstract

The axial and radial thermal responses of a cast-in place 10 m long energy pile and 0.6 m in diameter, installed in unsaturated sand under a 6-storey building, are examined during a heating-cooling cycle. The instrumentation in the pile was configured to compare radial and axial thermal responses at the same elevations and to evaluate the temperature and axial thermal stress distribution across the cross-sectional area of the pile. The magnitudes of the axial thermal strains were more constrained than the radial thermal strains at all depths, leading to the development of axial and radial thermal stresses of up to -4.5 MPa and -0.015 MPa, respectively, for a change in average pile temperature of 24.1°C. The magnitudes of the radial thermal stresses with changes in pile temperature were significantly lower than the axial thermal stresses at all depths of the pile, indicating that the radial thermal expansion had negligible effects on the development of axial thermal strains and stresses. The temperature distribution over the cross-section of the pile showed low variations at all depths, indicating that it would be justified to consider a uniform temperature distribution at least in piles of similar dimensions and with even heat exchanger layouts.

Keywords: *Energy piles; field tests; axial thermal response; radial thermal response; building loads.*

Introduction

Energy piles are foundation elements that act as both structural supports and underground heat exchangers to assist in maintaining thermal comfort in built structures when coupled with ground source heat pumps (Brandl, 2006; DeMoel et al., 2010; Bouazza et al., 2011). The temperatures in the energy pile vary according to the heating and cooling demands of the built structure, and the temperature changes induce additional axial and radial thermal stresses in the piles that can potentially affect the interaction between the energy piles and the soil. A pile-soil and pile-slab interaction assessment at a field-scale under real boundary conditions is an important component of improving the design and implementation of energy piles.

Numerical studies on the thermo-mechanical response of energy piles have shown that non-uniform temperature and axial thermal stress distributions tend to develop over the cross-section of the pile (Abdelaziz and Ozudogru, 2016a, 2016b; Caulk et al., 2016). Modelling approaches tend to utilize uniform pile temperatures with depth and across the cross-section of the pile when estimating axial thermal stresses (Pasten and Santamarina, 2014; Chen and McCartney, 2016). An assessment of temperature and stress distribution across the planar cross-section of the energy pile at a field-scale will provide much-needed insight into the complex temperature and stress response of concrete in a pile.

Recent studies on instrumented field scale-energy piles have mostly assessed their axial thermal responses (Laloui et al., 2006; Brandl, 2006; Bourne-Webb et al., 2009; McCartney and Murphy, 2012; Akrouch et al., 2014; Mimouni, 2014; Mimouni and Laloui, 2015; Wang et al., 2015; Murphy et al., 2015; Sutman et al., 2017; Murphy and McCartney, 2015; Faizal et al., 2016; You et al., 2016; McCartney and Murphy, 2017). However, only a few of these studies have been conducted under actual building loads with their outcomes reported in literature (Brandl, 2006, Laloui et al., 2006; Mimouni 2014; Mimouni and Laloui, 2015; Rotta Loria and Laloui, 2017, 2018, McCartney and Murphy, 2012; Murphy et al., 2015; Murphy and McCartney, 2015; Caulk et al., 2016; McCartney and Murphy, 2017). Assessment of energy piles under building loads can provide a better evluation of their thermo-mechanical response under real boundary conditions compared to controlled loading scenarios. Also, the current field-scale studies did not characterize the distribution in temperatures and axial thermal stresses across a planar cross-section of the energy pile needed to confirm the numerical simulations of Abdelaziz and Ozudogru (2016a, 2016b) and Caulk et al. (2016). Furthermore, consideration of the radial thermal responses in field-scale energy piles is limited to a few studies (Laloui et al., 2006; Amis et al., 2008; Mimouni, 2014; Mimouni and Laloui, 2015; Wang et al., 2015; Wang, 2017; Faizal et al. 2018). Limited analyses have been performed on the radial thermal responses along the length of the pile under building loads in these studies. The study by Wang et al., (2015) and Faizal et al. (2018) on an unrestrained 16.1 m long energy pile with a 0.6 m diameter installed in unsaturated dense sand has shown that axial thermal strains were more restricted to thermal expansion than radial thermal strains, where the radial thermal strains were indicated to be closer to that of a pile in free thermal expansion. On the other hand the study by Mimouni and Laloui (2015), on a 28 m long energy pile with 0.9 m diameter installed in a saturated in stiff bottom moraine and sandstone and under building loads showed that the radial thermal strains of the pile were much lower than the free thermal strains, indicating that stiffer soils provided higher restriction to radial thermal strains than the case reported by Wang et al. (2015) and Faizal et al. (2018). It is, therefore, possible that building loads could affect the development of radial thermal strains along the length of the pile. Furthermore, centrifuge-scale studies in unsaturated compacted silt have indicated that radial thermal expansion of energy piles during monotonic heating can possibly affect the ultimate capacity of the pile by mobilizing the radial pile-soil contact stresses

(McCartney and Rosenberg, 2011; Goode and McCartney, 2015). Further investigations on the axial and radial thermal strains along the length of the pile, particularly under building loads and installed in unsaturated media, are therefore required to assess the combined effects of axial and radial thermal expansion of the energy pile.

Due to the low diameter to length ratio of the pile, radial thermal effects are commonly considered to be relatively small in comparison to axial thermal effects when predicting the axial thermal response of energy piles (Knellwolf et al., 2011; Suryatriyastuti et al., 2014; Chen and McCartney, 2016). Some load transfer analysis methods have consistently validated and predicted the axial thermal response of field and centrifuge-scale energy piles by neglecting the radial thermal effects (Knellwolf et al., 2011; Chen and McCartney, 2016). Some numerical studies have also noted that radial thermal stresses in the energy pile are significantly low compared to the axial thermal stresses along the length of the pile (Gawecka et al., 2017; Ozudogru et al., 2015). These, however, require confirmation from field tests under building loads representing real boundary conditions.

The variations in pile-soil contact stresses in field-scale energy piles has mostly focussed on the assessment of side shear stresses resulting from axial thermal deformations of the pile (Bourne-Webb et al., 2009; Amatya et al. 2012; Bourne-Webb et al., 2013; Murphy et al., 2015; Murphy and McCartney 2015). Preliminary numerical and analytical studies on energy piles (Olgun et al., 2014; Zhou et al., 2016) along with a field study on an energy pile without end restraints (Faizal et al., 2018) have used cavity expansion analyses to confirm that no significant changes in pile-soil contact stresses are expected from the radial thermal expansion of the pile. These studies, however, need validation at various depths of a field-scale energy pile under building loads. Moreover, the thermally induced axial stresses in field-scale energy piles has been shown to significantly modify the axial mechanical loads in the pile imposed by the overlying structure (Laloui et al., 2006; Bourne-Webb et al., 2009; Murphy and McCartney, 2015; You et al., 2016; Sutman et al., 2017; McCartney and Murphy, 2017), but the effects of radial thermal stresses on the radial mechanical loads still needs to be investigated.

This paper aims to investigate the axial and radial thermal responses at different depths of a field-scale energy pile under building loads. The specific aims are to compare the axial and radial thermal responses along the length of the pile and to assess the temperature and axial thermal stress distribution over the planar cross-section of the energy pile at different depths. An instrumented field-scale energy pile installed under a recently constructed 6-storey student residential building was subjected to a heating-cooling cycle to investigate the objective of this study.

Ground Conditions

The ground conditions obtained from the site investigation report are summarized in Table 1.The site consisted of Tertiary age sedimentary deposits forming part of the Brighton Group, a common geological unit of Melbourne. These deposits typically comprise of shallow surface sands and silt underlain by moderate strength clays, and medium dense to dense clayey and silty sands with increasing depth. The fill material at the site was moist with a medium density and was comprised of crushed rock and/or silty sands up to a depth of 0.4 m. Underlying the fill material to a depth of approximately 3.5 m, the soil consisted of moist natural silty and sandy clay with stiff to very stiff consistency. Interbedded thin sandy lenses were also present up to this depth. Moist dense sand existed at a depth of approximately 3.5 m to 12.5 m. The sand consisted of interbedded layers of clayey sand and silty sand with the presence of cemented lenses. There was no groundwater encountered within the depth of the pile and the soil at the site is unsaturated. The thermal properties of the soil at the current site are expected to be similar to those reported for a field-scale energy pile site located in the same soil profile (i.e. unsaturated dense sand) at a distance of approximately 500 m from the current site (Barry-Macaulay et al., 2013; Singh et al., 2015; Yu et al., 2015; Faizal et al., 2018).

Energy Pile Details and Experimental Procedure

Two 0.6 m diameter cast-in-place bored piles with a length of 10 m and aspect (length to diameter) ratio of 16.7, from a set of up to 114 foundation piles for a new six-storey student residential building at Monash University, Melbourne, Australia, were converted to energy piles. A schematic of the layout of the piles under the building is shown in Fig. 1. The aspect ratio (16.7) of the energy pile in the current study is within the range of 10 to 50 commonly reported in literature (Loveridge and Powrie, 2013; Bourne-Webb et al., 2016). The size of the energy piles can vary largely within a building footprint or between different sites as these piles are dimensioned based on the local soil and structural load requirements. The diameters of energy piles can range from 0.15m to 3 m with lengths of 10 m to 60 m (Bourne-Webb et al., 2016), although smaller lengths of 5.5 m have also been studied (Akrouch et al., 2014). One of the two energy piles (Energy Pile 1 in Fig. 1) was instrumented with vibrating wire strain gauges (VWSGs) and thermocouples as described by in the schematic shown in Fig. 2, and is the only pile subjected to a heating-cooling cycle in this study. The pile reinforcement cage contained ten vertical reinforcement bars of 30 mm diameter, outer ring diameter of 445 mm made with 16 mm diameter rods which were spread spirally across the length of the pile cage at a spacing of 150 mm. Four U-loops of high-density polyethylene (HDPE) pipes with outer and inner diameters of 25 mm and 20 mm, respectively, were attached to the inside of the reinforcing cage of the pile using cable ties, shown in Fig. 3a. The nominal concrete cover to the edge of the pipes was 95 mm. The horizontal spacing between the pipes in a given U-loop was approximately 200 mm.

The HDPE pipes and sensors in the pile were installed before lowering the pile cage in the drilled hole. Then, concrete was slowly poured using removable PVC pipe tremies with 100 mm diameter to avoid damage to the sensors during free fall of the concrete. The concrete mix used consisted of 7 mm aggregated cement, slag, and fly ash with water to cement ratio of 0.42. The uniaxial compressive strength of unreinforced cylindrical concrete samples (100 mm diameter and 200 mm height) tested in the laboratory were 40 MPa and 62 MPa at 7 days and 33 days following the installation of the pile, respectively, with a modulus of elasticity of 34 GPa at 133 days following the installation of the pile.The instrumented energy pile contained 30 VWSGs (model Geokon 4200) installed at five depths of the pile. The axial VWSGs were installed at depths of 1 m (Level E), 3.05 m (Level D), 5 m (Level C), 7.28 m (Level B), and 9.5 m (Level A) below the ground surface. The radial VWSGs were installed at depths of 1.36 m (Level E), 3.3 m (Level D), 5.3 m (Level C), 7.46 m (Level B), and 9.25 m (Level A). The axial VWSGs at each level are referenced as V1, V2, V3, V4, and V5, whereas the radial VWSGs are referenced as R (e.g., AV1 corresponds to the axial VWSG at a depth of 9.5 m, AR corresponds to the radial VWSG at a depth of 9.25 m). At each of the five levels, there are four axially oriented VWSGs at a nominal concrete cover of 160 mm (i.e. V1, V2, V3, and V4), and an axially and radially oriented VWSG placed close to the centre of the pile (V5 and R, respectively) (Fig. 3b). The outer axial VWSGs were attached to the reinforcement bars, the central axial VWSGs were attached to the outer side of the tremie guides, and radial VWSGs were attached to steel bars welded across the diameter of the pile. The VWSGs were mounted on 30 mm high Styrofoam blocks to ensure that their orientations remain intact and that concrete strains are recorded and not that of steel. Type T thermocouples recorded the water temperatures at the inlet and outlet of each U-loop. The inlet and outlet of all the U-loops were connected to the inlet and outlet of the heating unit through a plumbing manifold. The heating unit, the data logging systems, and the plumbing manifold were placed on a 2 m raised mezzanine floor in a pump room 15 m away from the energy piles. The HDPE pipes from the energy piles to the pump room were run horizontally within the concrete slab of the building. All the pipes running from the exit of the concrete slab to the plumbing manifold were insulated. The water flow rates were recorded using TM series digital water flowmeters installed at the inlet and outlet of the plumbing manifold. Data from the thermocouples were logged using Pico Technology's USB-TC08 data loggers. Data from the VWSGs were logged using Campbell Scientific CR1000 data loggers. Data from three VWSGs were manually recorded at different operating times using a portable Geokon GK404 data logger due to synchronization issues with the CR1000 data logger.

The heating experiment was conducted for 18 days at a water flow rate of 11 litres per minute, followed by 50 days of cooling with natural ground recovery. The operating hours of GSHPs vary depending on the type of application. Residential buildings may require GSHP operation for certain hours per day leading to cyclic temperature changes of the pile, while some applications such as hospitals and commercial buildings may use the GSHP continuously for long term operations resulting in monotonic heating or cooling of the pile (Faizal et al., 2016). The present study focuses on the effects of monotonic heating of the energy pile which could also be considered as an extreme heating case as the inlet water temperatures were higher than the typical range of operating temperatures of 10°C to 35°C (Brandl, 2006; McCartney and Murphy, 2012; Murphy and McCartney, 2015; McCartney and Murphy, 2017). The water temperatures recorded at the inlet and exit of each U-loop at the pile head are shown in Fig. 4a. The four U-loops were connected in series; hence the temperature at the exit of each loop is similar to the inlet temperature of the consecutive loop. All the four U-loops were thermally active giving an even distribution of the heat exchanger layout in the pile. The water temperatures reduced from approximately 48°C to 44°C from the inlet of Loop 1 to the exit of Loop 4 during the heating period. The change in water temperatures between the inlet of U-loop one and the exit of each U-loop are shown in Fig. 4b. The difference in water temperatures increased from 1.5°C for one loop to 4.3°C for the four loops due to the increase in heat transfer area as water moves from the inlet of Loop 1 to the exit of Loop 4. Thermal performances of energy piles are better for higher number of U-loops due to higher heat exchange rates and also depend on the radius of the piles (Li et al. 2006; Hamada et al., 2007, Bourne-Webb et al., 2016).

Mechanisms of Thermal Response

The analysis and discussions of the results presented in this paper are based on the thermal response mechanisms of a pile restrained at both ends and subjected to heating, as shown in Fig. 5 (Bourne-Webb et al., 2009; Amatya et al., 2012; Bourne-Webb et al., 2013; Olgun et al., 2014; Faizal et al. 2018). The tensile and compressive stresses are considered as positive and negative, respectively.

The pile expands axially outwards from the null point where the thermal displacement is ideally zero, and the axial thermal stresses are maximum (Fig. 5a). The reaction forces or mobilized axial side shear stresses act in the opposite direction of expansion to maintain equilibrium, i.e. downward friction develops above the null point and upward friction develops below the null point. Compressive axial thermal stresses are developed in the pile due to the restraint provided by the surrounding soil and the pile ends. The pile expands radially outward from the centre of the pile and is restrained by the surrounding soil, leading to the development of compressive radial thermal stresses in the pile (Fig. 5b). The reactive forces from the surrounding soil or the radial pile-soil contact stresses are equal and opposite to that induced by the radial thermal expansion of the pile to maintain radial stress equilibrium.

Results and Discussions

Time Series of Temperatures and Thermal Strains

The thermal strains measured using the vibrating wire strain gauges were corrected for temperature effects as follows:

$$\varepsilon_T = (\varepsilon_i - \varepsilon_o)B + (T_i - T_o)\alpha_s \tag{1}$$

where ε_i is strain at time *i*, ε_o is the reference strain, *B* is the batch calibration factor of the strain gauges with a magnitude of 0.975, T_i is the temperature of the strain gauges at time *i*, T_o is the reference temperature of the strain gauges, α_s is the coefficient of linear thermal expansion of steel wire in the strain gauges (12.2 με /°C). The value of ε_o was selected at the beginning of the experiment and thus the calculated thermal strains neglects the effects of any strains due to the weight of the building. The axial and radial thermal strains and stresses were isolated and analyzed separately from that due to building loads. The strains ε_i and ε_o were calculated as follows:

$$\varepsilon = G(f^2 \times 10^{-3}) \tag{2}$$

where *f* is the resonant frequency of the strain gauges at the reference or at time *i*, and *G* is the gauge factor with a magnitude of 3.304.

The time series of the temperatures and thermal strains developed in the pile during heating and cooling are shown in Fig. 6. Average magnitudes of the thermal responses from the axial VWSGs at a given depth were considered for ease of comparison with the radial thermal responses at that depth. The radial VWSG at a depth of 1.36 m was damaged before the experiment and did not give feedback on the radial thermal strains. The pile temperatures and change in pile temperatures with respect to initial conditions recorded from the axial and radial VWSGs showed similar magnitudes, as shown in Fig. 6a to Fig. 6d. The pile temperatures recovered to near initial temperatures at the end of the 50 days of natural ground cooling.

The time series of the axial and radial thermal strains shown in Fig. 6e and Fig. 6f, respectively, had large differences in magnitudes. Also, the strains recovered to near initial conditions at the end of cooling, indicating a thermo-elastic response of the energy pile. The thermo-elastic response of the energy pile is further confirmed by the plots of the axial and radial thermal strains against the change in pile temperatures, shown in Fig. 6g and Fig. 6h, respectively. The axial and radial thermal strains follow almost reversible linear paths against the change in pile temperatures during both heating and cooling at all depths. The radial thermal strains are slightly offset in the last few days of cooling possibly due to slight fluctuations in pile temperatures during recovery. The linear reversible paths of the thermal strains indicate that the pile temperature changes coupled with the load of the building did not lead to significant thermally induced pile and soil deformations for the short term heating and cooling studied.

Evaluation of Thermal Responses against Depth

The thermal stresses developed in the pile were estimated using the difference between the free and restricted thermal expansions, as follows (Amatya et al., 2012; Murphy et al., 2015; Caulk et al., 2016):

$$\sigma_T = E_p(\alpha_{mobilized} - \alpha_{free})\Delta T \quad (3)$$

where E_p is the Young's modulus of the concrete, $\alpha_{mobilized}$ is the thermal expansion coefficient of the concrete restrained by the pile-soil interaction and is calculated by dividing the thermal strains, ε_T, by the change in pile temperatures with respect to initial conditions, ΔT, and α_{free} is the free or unrestrained thermal expansion coefficient of the concrete. An average value of α_{free} = 13 με /°C was considered and was slightly adjusted within ± 1 με /°C to confirm that the magnitudes of the radial thermal stresses developed in the pile are equal to the pile-soil radial contact stresses (i.e. $\sigma_n = \sigma_T$ for radial stress equilibrium (Fig. 5b). The coefficient of linear thermal expansion of concrete has been reported to range from 9 με/°C to 14.5 με/°C depending on the aggregate mineralogy of the concrete mix (Stewart and McCartney, 2014).

The profiles of axial and radial thermal responses with depth during the heating period are compared in Fig. 7. These profiles are drawn at approximately 5°C intervals of the change in average pile temperatures of all the VWSGs in the pile, ΔT_{ave}, at a given operating time. The ΔT_{ave} magnitudes considered are 0°C, 5.3°C, 10.1°C, 15°C, 20.1°C, and 24.1°C corresponding to 0, 6.8, 16, 38, 128, and 432 hours of operation, respectively.

The pile temperatures shown in Fig. 7a and Fig. 7b reached up to 45°C at end of heating with a maximum change in pile temperatures of approximately 25°C with respect to initial conditions, shown in Fig. 7c and Fig. 7d. The magnitudes of the thermal strains (Fig. 7e and Fig. 7f) and the thermal stresses (Fig. 7g and Fig. 7h) increased with increasing ΔT_{ave}. The lowest axial thermal strains in Fig. 7e, and hence the largest axial thermal stresses in Fig. 7f, is at a depth of 3.05 m and can be stated as the location of the null point. The position of the null point at this depth indicates that the overlying structure imposes a higher stiffness at the pile head compared to the stiffness imposed by the base resistance at the toe.

Due to large differences in magnitudes between the axial and radial thermal strains, the radial thermal stresses are significantly lower than the axial thermal stresses at all depths. The magnitudes of axial and radial thermal stresses are up to -4.5 MPa and -0.015 MPa, respectively, at the null point for ΔT_{ave} = 24.1°C. Significantly lower magnitudes of radial thermal stresses compared to axial thermal stresses have also been observed in numerical studies on energy piles (Gawecka et al., 2017; Ozudogru et al., 2015) and a field-scale study (Faizal et al., 2018) The implication of the large differences between the magnitudes of the axial and radial thermal stresses in the present study are that the mobilization of the pile-contact stresses was not significantly affected due to the radial thermal expansion of the pile, as shown in Fig. 9 and Fig. 10.

The magnitudes of radial thermal strains and stresses, shown in Fig. 7f and Fig. 7h, respectively, are relatively uniform at all depths for any given ΔT_{ave}, indicating that the soil formation at the site provides a similar restriction to radial thermal expansion at all depths. The axial thermal strains and stresses, however, show varying magnitudes along the depth of the pile for any given ΔT_{ave}. The implication of this difference is that the development of axial thermal strains and stresses, and hence the location of the null point, depends on the restrictions imposed by the surrounding soil as well as by the pile ends, while the radial thermal strains and stresses develop mostly from the restriction by the surrounding soil. Furthermore, the very low magnitudes of radial thermal stresses indicate that the restrictions to the radial thermal expansion of the energy pile do not contribute to the development of axial thermal strains and stresses along the length of the pile.

The load transfer analysis conducted by Chen and McCartney (2016) had also indicated that radial thermal expansion of the pile has negligible influence on the development of axial thermal strains and stresses. The field study on an unrestrained bored energy pile, with a 0.6 m diameter and 16.1 m length, conducted by Wang et al., (2015) and Faizal et al., (2018) showed that the axial thermal strains were more restricted to thermal expansion than the radial thermal strains, where the radial thermal strains were indicated to be closer to that of a pile in free thermal expansion. The energy pile studied by Wang et al., (2015) and Faizal et al., (2018) was installed approximately 500 m from the site described in the current paper. The soil formations at these two sites are similar and consist of dense to very dense unsaturated sands. The field study by Mimouni and Laloui (2015), however, showed that radial thermal strains could experience high restriction to thermal expansion in very stiff soil layers causing the axial thermal expansions to increase. They assessed the heating effects on the axial and radial thermal strains in a field-scale bored energy pile, with a diameter of 0.9 m and a length of 28 m, installed under a water retention tank in saturated soil. The radial thermal strains at a depth of 19 m in stiff bottom moraine and sandstone were restricted entirely to thermal expansion, and it was concluded that this restriction led to higher axial thermal expansions at the lower part of the pile between the depths of 22 m to 28 m. The differences in thermal response between the current study and that presented by Mimouni and Laloui (2015) could be due to differences in pile construction techniques, different soil properties, and differences in pile geometries, and is not likely due to the differences in building loads at the pile head. For example, the 0.9 m pile diameter in the Mimouni and Laloui (2015) study would experience larger thermal effects than the 0.6 m pile diameter in the present study and the study reported by Wang et al., (2015) and Faizal et al., (2018).

Evaluation of Thermal Expansion

The axial and radial thermal expansion coefficients of the concrete restrained by the interaction between the pile and the soil, $\alpha_{mobilized}$ coefficients, are shown in Fig. 8a.

The axial and radial $\alpha_{mobilized}$ coefficients ranged between 7.2 με/°C to 9.6 με/°C and 12.3 με/°C to 13.3 με /°C, respectively, between the different depths, with the magnitudes of the radial $\alpha_{mobilized}$ coefficients being closer to the magnitudes of the thermal expansion coefficient of concrete in free or unrestrained expansion. This indicates that the surrounding soil provides minimal restriciton to the radial thermal strains at all depths compared to the large restrictions to axial thermal strains, thus further confirming that radial thermal expansion of the pile is not expected to contribute to the development of axial thermal stresses in the energy pile at all depths in the current study. The radial thermal strains were also reported to be closer to free thermal expansion in the numerical study by Olgun et al. (2014) in cohesive soil and in the field study by Wang et al. (2015) and Faizal et al. (2018) in a soil formation similar to the site in this paper.

The ratios of the axial to radial thermal strains are plotted against the midpoint between axial and radial VWSGs, shown in Fig. 8b. The magnitudes of strain ratios vary with depth, due to the differences in restrictions to thermal expansions of mostly the axial thermal strains, with the lowest magnitude of approximately 0.54 being near the location of the null point. The variations in strain ratios with depth in Fig. 8b indicates that the thermally induced volumetric expansion of the pile varies with depth. Even though there was a loss of radial thermal strain data at a depth of 1.36 m, thus the strain ratio is unknown at this depth, the lowest volumetric expansion of the energy pile would still be expected to be at the location of the null point in this study due to the largest restrictions in axial thermal strains and development of largest thermal stresses at the null point, as described for Fig. 5a, Fig. 7e and Fig. 7g.

Pile-soil Contact Stresses

The side shear stresses mobilized by the axial thermal expansion of the pile, τ_{TA}, were estimated from the differences in axial thermal stresses at the midpoint of two axial VWSGs, and assuming that the modulus of elasticity is constant along the length of the pile. τ_{TA} is given as follows (Laloui, 2011; Murphy et al., 2015; Murphy and McCartney, 2015):

$$\tau_{TA} = \frac{(\sigma_{TA,j} - \sigma_{TA,j-1})D}{4\Delta l} \quad (4)$$

where *D* is the pile diameter, *j* is the location of the axial VWSGs and *Δl* is the distance between the axial VWSGs. The mobilized radial contact stresses, σ_n, resulting from the radial thermal expansion of the pile were estimated using a cavity expansion analysis, given as follows:

$$\sigma_n = \frac{E_s}{1+v_s} \frac{\Delta r}{r} \quad (5)$$

where E_s and v_s are the Young's modulus and Poisson's ratio of the surrounding dense sand (assumed to be 60 MPa and 0.3, respectively, based on typical values for dense sand), r is the pile radius, and Δr is the thermally induced radial displacement of the pile (Δr/r is assumed to be equal to the radial thermal strain for a given change in temperature). This simple model assuming a constant stiffness is considered useful for analysing the radial pile-soil contact stresses since the shear strength of sand is not expected to be affected by temperature variations (Barry-Macaulay, 2013; Di Donna et al., 2015; Yavari et al., 2016) and the thermally induced change in pile radius, Δr, is relatively small compared to the initial pile radius. Also, the reversible axial and radial thermal strains in Fig. 6 shows a thermo-elastic response of the pile which indicates that no significant irreversible changes occurred at the pile-soil interface for the range of temperatures studied.

The contact stresses shown in Fig. 9 increased with increasing ΔT_{ave} as the pile underwent higher thermal expansion. The thermally induced side shear stresses mobilized by the axial thermal expansion of the pile, shown in Fig. 9a, change direction at the null point, with downward or negative side shear stresses above the null point and upward or positive side shear stresses below the null point. The magnitudes of the thermally induced side shear stresses in Fig. 9a vary with depth due to variations in axial thermal strains and stresses, whereas the thermally induced radial contact stresses shown in Fig. 9b are relatively uniform across the length of the pile since the radial thermal strains and stresses are relatively uniform. There is a lower change in axial thermal stresses between the depths of 5 m to 7.28 m (Fig. 7g) leading to lower changes in side shear stresses. The non-linearity in distribution of axial thermal stresses (Fig. 7g) and the side shear stresses (Fig 9a) with depth becomes more significant for higher temperatures (i.e. above 15°C) due to higher resistance from the soil and pile ends to thermal expansion of the pile.

The largest thermally induced side shear stress magnitude above the null point is -81 kPa and 71 kPa below the null point for ΔT_{ave} = 24.1°C. The largest magnitude of thermally induced radial contact stresses is comparatively lower than the side shear stresses and is up to 15.3 kPa for ΔT_{ave} = 24.1°C. Low magnitudes of radial contact stresses due to radial thermal expansion of the pile, up to 15 kPa, were reported by Olgun et al. (2014) for a pile temperature change of up to 10°C in cohesive soil and up to 12 kPa by Faizal et al. (2018) for a pile temperature change of 22.5°C for a pile without end restraints and installed in a similar soil profile to the present study. The range of magnitudes of radial contact stresses in the present study and in the study of Faizal et al., (2018) are similar, indicating that the axial mechanical load at the pile head in the present study does not have any significant effects on the mobilization of radial pile-contact stresses. The differences in the magnitudes of the contact stresses indicate that the large axial thermal stresses developed in the pile are more dominant in mobilizing the side shear stresses than the radial thermal stresses are in mobilizing the radial contact stresses at all depths, hence the changes in radial contact stresses may not significantly affect the changes in the overall pile-soil contact stresses due to temperature-induced volumetric changes of the energy pile.

Thermal Responses to Change in Pile Temperatures

The axial and radial thermal responses of the pile for all depths against the respective change in pile temperatures obtained from the VWSGs, ΔT, up to Day 18 of the experiment are compared in Fig. 10.

The lowest magnitude of the axial thermal strain for a given change in pile temperature is 7.35 με/°C at a depth of 3.05 m at the null point, shown in Fig. 10a, compared to radial thermal strain of 12.68 με/°C at a nearby depth of 3.3 m, shown in Fig. 10b; the radial thermal strains are approximately 73% higher than the axial thermal strains at the null point. The large differences in thermal strains at the null point lead to the development of the large axial thermal stress magnitude of -181.81 kPa/°C at the null point, shown in Fig. 10c, compared to negligible magnitudes of radial thermal stresses of ≈ -0.59 kPa/°C for all depths, shown in Fig. 10d. The slope of the radial contact stresses mobilized by the radial thermal expansion of the pile, shown in Fig. 10f, is also much lower than the side shear stresses mobilized by the axial thermal expansion of the pile, shown in Fig. 10e. The highest side shear stress magnitude of -3.28 kPa/°C is near the pile head compared to ≈ 0.59 kPa/°C radial contact stresses along the length of the pile. The results indicate that the radial thermal effects are significantly lower compared to the thermal axial effects at all depths of the energy pile. The radial thermal effects are lower than the axial thermal effects possibly due to the small magnitude of the ratio of the pile diameter to the pile length (i.e. 0.06) as well as the particular construction effects associated with bored cast-in-place piles where the density of the soil on the borehole wall is not significantly modified compared to driven piles (Ng et al., 2016).

The magnitudes of the slopes of axial thermal responses against change in pile temperatures vary with depth, whereas the slopes of the radial thermal responses are similar for all depths. This observation confirms that temperature changes lead to a coupled effect of the pile end and side restraints on the development of axial thermal responses along the length of the pile, whereas the radial thermal responses appear to develop mostly due to the restrictions from the surrounding soil with negligible effects from the pile end restraints.

The implication of the large differences between the axial and radial thermal responses against change in pile temperatures is that the radial thermal effects will remain significantly lower and negligible in comparison to the axial thermal responses along the length of the pile for the commonly encountered operating temperatures in cast-in-place energy piles installed in dense sand. The radial thermal expansion of the energy pile is therefore not expected to contribute significantly to the development of axial thermal stresses in the pile and to the changes in contact stresses at the pile-soil interface at all depths. These results confirm the recommendations of load transfer analyses that had consistently validated the axial thermal responses of field and centrifuge-scale energy piles by neglecting the radial thermal effects (Knellwolf et al., 2011; Chen and McCartney, 2016).

Thermo-mechanical Stresses

The comparison of axial and radial thermal stresses with the respective mechanical stresses in the pile imposed by the overlying structure is shown in Fig. 11. The mechanical stresses are evaluated from the changes in strains recorded during building construction multiplied by the modulus of elasticity of the pile. The thermo-mechanical stresses are the sum of the thermal and mechanical stresses. The design compressive and tension axial working mechanical loads of the 10 m long, 600 mm diameter pile were 1404 kN (4.96 MPa) and 1122 kN (3.97 MPa), respectively. The ultimate capacities of compressive and tension mechanical loads with a factor of 1.9 were 2701 KN (9.6 MPa) and 2157 KN (7.6 MPa), respectively. The design pile head load is thus approximately 52% of the calculated ultimate pile head load of the instrumented energy pile.

The thermal stresses shown in Fig. 7g and Fig. 7h are re-plotted in Fig. 11a and Fig.11c, respectively, to compare their magnitudes with the magnitudes of mechanical stresses in the pile. The axial thermal stresses in Fig. 11a increased with increasing ΔT_{ave} and exceeded the mechanical stresses at ΔT_{ave} = 24.1°C. The largest magnitude of the axial thermo-mechanical stress was -8.5 MPa, for ΔT_{ave} = 24.1°C at the end of the experiment and is within the magnitudes of the compressive strength and the ultimate capacity of the pile. The axial thermal stresses were much higher than the axial mechanical stresses near the toe of the pile for high temperatures due to high base resistance from the dense sand at the base of the pile. Similar trends of axial thermo-mechanical stresses for a field-scale energy pile was also reported by Laloui et al. (2006).

The typical operating temperatures of energy piles range from 10°C to 35°C depending on the usage requirements (Brandl, 2006; McCartney and Murphy, 2012; Murphy and McCartney, 2015; McCartney and Murphy, 2017) resulting in average pile temperature changes of up to 15°C which is the value normally encountered for heat exchanger piles (Laloui et al, 2006). The maximum magnitudes of axial thermo-mechanical stress for ΔT_{ave} = 15°C in Fig. 11b is approximately -6.4 MPa and is considerably lower than the ultimate capacity of the pile. The magnitudes of radial thermal stresses shown in Figure 11c are negligible in comparison to the radial mechanical stresses, hence very minimal changes occur in the overall radial thermo-mechanical stresses shown in Figure 11d. The results further confirm that radial thermal effects developed in the energy pile are negligible in comparison to axial thermal effects.

Cross-sectional Distribution of Temperatures and Axial Thermal Stresses

The distribution of pile temperatures and axial thermal stresses obtained from the individual axial VWSGs over the planar cross-section of the energy pile at all depths are shown in Fig. 12, and Fig. 13, respectively. The locations of the axial VWSGs are non-dimensionalized with respect to the radius of the pile. The axial VWSGs at locations V1 and V2, shown in Fig. 2, correspond to the non-dimensional radius of -0.47, V5 corresponds to the centre of the pile, and V3 and V4 correspond to the non-dimensional radius of 0.47. The results are presented at average pile temperatures of 5.3°C, 15°C, and 24.1°C, corresponding to low, commonly expected, and above commonly expected temperatures in energy piles. The operating times corresponding to these average pile temperatures are 6.8 hours, 38 hours, and 432 hours, respectively.

The pile temperatures shown in Fig. 12 increases with increasing average change of pile temperatures and reach up to 45°C at all depths. There is a temperature variation of up to 3.7°C for all operating times at a depth of 9.5 m, shown in Fig. 12e, possibly due to the cluster of HDPE pipe U-bends near the base of the pile causing larger temperature differences due to increase in turbulence of the water in the pipes. The pile temperatures at other depths are in the low range of temperature and varieds between 0.6°C to 1.5°C. This low range of temperature variations over the cross-section of the pile indicates that it would be justified to consider uniform temperatures over the planar cross-section of the pile for designing energy piles with an even layout of heat exchangers and with similar pile dimensions, thermo-mechanical loads and soil conditions. There are slight variations in temperatures possibly due to differences in thermal properties of the different materials in the concrete mix. Uniform temperatures were observed for all the three operating hours presented during monotonic heating, indicating that the pile reached a uniform temperature distribution across the cross-section even for a short duration of operation of 6.8 hours. Further studies are required to assess the temperature distributions for intermittent operations where the energy pile operates for certain hours per day leading to frequent cyclic temperature changes of the pile.

The axial thermal stress distribution over the planar cross-section of the energy pile is shown in Fig. 13. The largest variations in axial thermal stresses were near the pile head at a depth of 1 m. The variations increased with increasing pile temperatures and reached up to a range of 3.3 MPa for ΔT_{ave} = 24.1°C. The pile toe at a depth of 9.5 m, however, had a comparatively lower axial thermal stress distribution. This could be attributed to the increased resistance to thermal expansion at the pile head due to higher stiffness provided by the overlying structure for high temperatures compared to the base of the pile, as discussed for Fig. 7g. The largest range of axial thermal stresses was 1.4 MPa, 0.6 MPa, 0.5 MPa, and 1 MPa at depths of 3.05 m, 5 m, 7.28 m, and 1 m, respectively. The effects of the overlying structure may have also caused additional variations in axial thermal stresses at a depth of 3.05 m compared to other depths. The soil-pile interaction combined with the pile head restraints from superstructure loads would ideally affect the axial stress distribution in the pile from the head of the pile to the location of the null point, while the soil-pile interaction and the restraints at the pile toe would ideally affect the axial stress distribution from the null point to the toe of the pile (Fig. 5).

The results of Fig. 13 indicate that pile end restraints will affect the axial stress distributions over the cross-sectional area near the pile ends, where higher stiffness provided by the overlying structure will induce more significant variations due to the pile-slab interaction and should be accounted for when designing energy pile systems. The upward axial thermal expansion of the energy pile head above the null point acts against the rigid concrete slab at the pile-slab joint and induces reactive stresses in the slab since the rigid slab prevents the energy pile head from expanding upward. These reactive stresses in the concrete slab, together with the axial thermal stresses in the pile near the pile head, need to be monitored in future field-scale studies to evaluate the pile-slab interaction effects better. The pile head heave against the slab could have increased the non-uniformity of the axial thermal stress distribution over the planar cross-section of the energy pile near the pile head. The non-uniformity of axial thermal stress distribution near the pile head could be larger for higher diameter piles due to higher area of contact between the pile head and the slab and is a subject for further studies. The thermal effects in the slab at the head of the energy pile could also lead to thermally induced deformations of the surrounding closely spaced piles that are linked with the energy pile through the rigid slab (i.e. group effects) (Di Donna et al., 2016; Rotta Loria and Laloui, 2017, 2018), hence further investigation is required on the axial and radial thermal responses of energy piles operating in a group.

Furthermore, the magnitudes of axial thermal stresses at the centre of the pile are different compared to the radial locations of ± 0.47. The axial thermal stresses near the pile head have lower magnitudes at the centre of the cross-section compared to the other radial locations. This could also be attributed to the pile-slab interaction effects which increase the non-uniformity of the axial thermal stress distribution at that location. The stress magnitudes below a depth of 5 m tend to show larger magnitudes at the centre of the pile, indicating that the centre of the pile is more constrained to axial thermal expansion compared to other radial locations.

The magnitudes of the axial thermal stresses at any location over the cross-section of the pile are well below the compressive strength of the concrete (62 MPa), and thus the non-uniform distribution of axial thermal stresses are not expected to affect the structural integrity of the pile for the studied case. . Even though not expected in reinforced piled foundations, further investigations are still warranted to assess the possibilities of concrete cracking due to differential expansions in a given cross-sectional area of the energy pile for the range of operating temperatures encountered in energy piles. The temperature and axial thermal stress distribution reported herein are for an even distribution of 4 HDPE pipe U-loops in the pile. Uneven distribution of U-loops could increase the non-uniformity of the pile temperatures and the axial thermal stress distribution over the cross-section of the pile (Caulk et al., 2016).

Conclusions

This study investigated the axial and radial thermal responses of a single cast-in-place bored energy pile installed in unsaturated dense sand under a six storey building. The energy pile, which had a diameter of 0.6 m and a length of 10 m (aspect ratio of 16.7), a pile design to ultimate load ratio of 52% and with even heat exchanger distribution in the pile, was subjected to monotonic heating with an average pile temperature change of 24.1°C. The thermal strains returned to near initial conditions at the end of the recovery period, indicating that the pile and the soil thermal response is elastic and that the temperature changes of the pile and the surrounding unsaturated dense sand did not affect the structural and geotechnical performance of the pile for the studied case. The magnitudes of radial thermal stresses were upto -0.015 MPa and were significantly lower than the axial thermal stresses which were upto -4.5 MPa indicating that the radial thermal expansion of the pile did not significantly modify the soil-structure interaction and did not contribute significantly to the development of axial thermal stresses along the length of the pile. The temperature distribution over the planar cross-section of the pile showed a low range of variations at all depths, indicating that it would be justified to consider uniform temperatures over the cross section when designing energy piles with similar structural and geotechnical characteristics to that studied in this paper. The axial thermal stresses also showed a low range of stress variations across the cross-section of the pile with magnitudes well below the compressive strength of concrete. Pile-slab interaction effects were found to induce larger variations in the cross-sectional distribution of the axial thermal stresses near the pile head compared to other depths and thus should be accounted for when designing energy pile systems. Finally, the results and conclusions of this study are specific to the studied site and may be applicable for energy piles with similar dimensions, loading and soil conditions as to those studied in this paper. Further studies are required on the evaluation of axial and radial thermal responses under other commonly encountered conditions at a field-scale, such as group effects, piles of different aspect ratios and different loading conditions, effect of soil types and saturation, and effects of cyclic temperature changes of the pile.

Acknowledgements

This research project is supported under the Australian Research Council's Linkage Projects funding scheme (project number LP120200613). The authors also acknowledge the Australian Government Research Training Program Scholarship provided to the first author. US National Science Foundation grant CMMI-0928159 supported the third author. The support of all the sponsors is gratefully acknowledged.

References

Abdelaziz, S. L. and Ozudogru, T. Y. (2016a). "Selection of the design temperature change for energy piles." *Applied Thermal Engineering*, 107(2016), 1036-1045.

Abdelaziz, S. and Ozudogru, T.Y. (2016b). "Non-uniform thermal strains and stresses in energy piles." *Environmental Geotechnics*, 3(4), 237-252.

Akrouch, G., Sánchez, M. and Briaud, J-L. (2014). "Thermo-mechanical behavior of energy piles in high plasticity clays." *Acta Geotechnica*, 9(3), 399-412.

Amatya, B. L., Soga, K., Bourne-Webb, P. J., Amis, T. and Laloui, L. (2012). "Thermo-mechanical behaviour of energy piles." *Géotechnique*, 62(6), 503-519.

Amis, T., Bourne-Webb, P., Davidson, C., Amatya, B., and Soga, K. (2008). "The effects of heating and cooling energy piles under working load at Lambeth College, UK." 33rd Annual and 11th Intl. Conf. of the Deep Foundations Institute, New York, USA.

Barry-Macaulay, D. (2013). "An investigation on the thermal and thermo-mechanical behaviour of soils." Master of Engineering Thesis, Department of Civil Engineering, Monash University, Melbourne, Australia.

Barry-Macaulay, D., Bouazza, A., Singh, R. M., Wang, B. and Ranjith, P. G. (2013). "Thermal conductivity of soils and rocks from the Melbourne (Australia) region." *Engineering Geology*, 164, 131-138.

Bourne-Webb, P. J., Amatya, B., Soga, K., Amis, T., Davidson, C. and Payne, P. (2009). "Energy pile test at Lambeth College, London: geotechnical and thermodynamic aspects of pile response to heat cycles." *Géotechnique*, 59(3), 237-248.

Bourne-Webb, P.J., Burlon, S., Javed, S., Kurten, S and Loveridge, F. (2016). Analysis and design methods for energy geostructures. *Renewable and Sustainable Energy Reviews*, 65, 402-419.

Bourne-Webb, P. J., Amatya, B., and Soga, K. (2013). “A framework for understanding energy pile behaviour.” *Proceedings of the Institution of Civil Engineers - Geotechnical Engineering*, 166(2), 170-177.

Brandl, H. (2006). “Energy foundations and other thermo-active ground structures.” *Géotechnique*, 56(2), 81-122.

Bouazza, A., Singh, R.M., Wang, B., Barry-Macaulay, D., Haberfield, C., Chapman, G., Baycan, S. and Carden, Y. (2011). “Harnessing on site renewable energy through pile foundations.” *Australian Geomechanics*, 46(4), 79-89.

Caulk, R., Ghazanfari, E., and McCartney, J.S. (2016). “Parameterization of a calibrated geothermal energy pile model.” *Geomechanics for Energy and the Environment*, 5(3), 1-15.

Chen, D. and McCartney, J.S. (2016). “Parameters for load transfer analysis of energy piles in uniform nonplastic soils.” *International Journal of Geomechanics*, 17 (7), 10.1061/(ASCE)GM.1943-5622.0000873, 04016159-1-17.

Di Donna, A., Ferrari, A., and Laloui, L. (2015). “Experimental investigations of the soil–concrete interface: physical mechanisms, cyclic mobilization, and behaviour at different temperatures.” *Canadian Geotechnical Journal*, 53(4), 659-672.

Di Donna, A., Rotta Loria, A. F., and Laloui, L. (2016). “Numerical study of the response of a group of energy piles under different combinations of thermo-mechanical loads.” *Computers and Geotechnics*, 72, 126-142.

De Moel, M., Bach, P. M., Bouazza, A., Singh, R. M., and Sun, J. O. (2010). “Technological advances and applications of geothermal energy pile foundations and their feasibility in Australia.” *Renewable and Sustainable Energy Reviews*, 14(9), 2683-2696.

Faizal, M., Bouazza, A. and Singh, R. M. (2016). “An experimental investigation of the influence of intermittent and continuous operating modes on the thermal behaviour of a full scale geothermal energy pile." *Geomechanics for Energy and the Environment*, 8, 8-29.

Faizal, M., Bouazza, A., Haberfield, C. and McCartney, J.S. (2018). "Axial and radial thermal responses of a field scale energy pile under monotonic and cyclic temperature changes". *Journal of Geotechnical and Geoenvironmental Engineering*, under review.

Gawecka, K. A., Taborda, D. M. G., Potts, D. M., Cui, W., Zdravković, L., and Kasri, M. S. H. (2017). "Numerical modelling of thermo-active piles in London Clay." *Proceedings of the Institution of Civil Engineers - Geotechnical Engineering*, 170(3), 201-219.

Goode, J. C. and McCartney, J. S. (2015). "Centrifuge modeling of end-restraint effects in energy foundations." *Journal of Geotechnical and Geoenvironmental Engineering*, 10.1061/(ASCE)GT.1943-5606.0001333, 04015034-1-13.

Knellwolf, C., Peron, H., and Laloui, L. (2011). "Geotechnical analysis of heat exchanger piles." *Journal of Geotechnical and Geoenvironmental Engineering*, 130 (10), 10.1061/(ASCE)GT.1943-5606.0000513, 890–902.

Hamada, Y., Saitoh, H., Nakamura, M., Kubota, H., and Ochifuji, K. (2007). "Field performance of an energy pile system for space heating." *Energy and Buildings*, 39(5), 517-524.

Laloui, L., Nuth, M. and Vulliet, L. (2006). "Experimental and numerical investigations of the behaviour of a heat exchanger pile." *International Journal for Numerical and Analytical Methods in Geomechanics*, 30(8), 763-781.

Laloui, L. (2011). "In-situ testing of a heat exchanger pile". *Geo-Frontiers 2011*, ASCE, Texas, United States, 410 – 419.

Li, X., Chen, Y., Chen, Z., and Zhao, J. (2006). "Thermal performances of different types of underground heat exchangers." *Energy and Buildings*, 38(5), 543-547.

Loveridge, F. and Powrie, W. (2013). “Pile heat exchangers: thermal behaviour and interactions.” *Geotechnical Engineering*, 166(2), 178–196.

McCartney, J.S. and Murphy, K.D. (2012). “Strain distributions in full-scale energy foundations.” *DFI Journal: The Journal of the Deep Foundations Institute*, 6(2), 26-38.

McCartney, J.S. and Murphy, K.D. (2017). “Investigation of potential dragdown/uplift effects on energy piles.” *Geomechanics for Energy and the Environment*, 10, 21-28.

McCartney, J.S. and Rosenberg, J. E. (2011). “Impact of heat exchange on side shear in thermo-active foundations.” *Geo-Frontiers 2011*, ASCE, Texas, United States, 488-498.

Mimouni, T. (2014). “Thermomechanical characterization of energy geostructures with emphasis on energy piles.” PhD thesis, Laboratory of Soil Mechanics, École Polytechnique Fédérale de Lausanne, Lausanne, Switzerland.

Mimouni, T. and Laloui, L. (2015). “Behaviour of a group of energy piles.” *Canadian Geotechnical Journal*, 52(12), 1913-1929.

Murphy, K. D. and McCartney, J. S. (2015). “Seasonal response of energy foundations during building operation.” *Geotechnical and Geological Engineering*, 33(2), 343-356.

Murphy, K. D., McCartney, J. S., and Henry, K. S. (2015). “Evaluation of thermo-mechanical and thermal behavior of full-scale energy foundations.” *Acta Geotechnica,* 10(2), 179-195.

Ng, C. W. W., Gunawan, A., Shi, C., Ma, Q. J., and Liu, H. L. (2016). “Centrifuge modelling of displacement and replacement energy piles constructed in saturated sand: a comparative study.” *Géotechnique Letters*, 6(1), 34-38.

Olgun, C.G., Ozudogru, T. Y. and Arson, C. F. (2014). “Thermo-mechanical radial expansion of heat exchanger piles and possible effects on contact pressures at pile–soil interface.” *Géotechnique Letters*, 4(3), 170-178.

Ozudogru, T.Y., Olgun, C.G., and Arson, C.F. (2015). “Analysis of friction induced thermo-mechanical stresses on a heat exchanger pile in isothermal soil.” *Geotechnical and Geological Engineering*, 33(2), 357-371.

Pasten, C., and Santamarina, J. (2014). “Thermally induced long-term displacement of thermoactive piles.” *Journal of Geotechnical and Geoenvironmental Engineering,* 10.1061/(ASCE)GT.1943-5606.0001092, 06014003-1-5.

Rotta Loria, A. F. & Laloui, L. (2017). “Thermally induced group effects among energy piles”. *Géotechnique* 67(5), 374–393

Rotta Loria, A. F. & Laloui, L. (2018) “Group action effects caused by various operating energy piles”.*Géotechnique*, 68(9), 834-841.

Singh, R., Bouazza, A. and Wang, B. (2015). “Near-field ground thermal response to heating of a geothermal energy pile: observations from a field test.” *Soils and Foundations*, 55(6), 1412-1426.

Stewart, M. A. and McCartney, J. S. (2014). “Centrifuge modeling of soil-structure interaction in energy foundations.” *Journal of Geotechnical and Geoenvironmental Engineering*, 10.1061/(ASCE)GT.1943-5606.0001061, 04013044-1-11.

Suryatriyastuti, M. E., Mroueh, H., and Burlon, S. (2014). “A load transfer approach for studying the cyclic behavior of thermo-active piles.” *Computers and Geotechnics*, 55 (2014) 378–391.

Sutman, M., Olgun, G., Laloui, L., and Brettmann, T. (2017). "Effect of end-restraint conditions on energy pile behavior." *Geotechnical Frontiers 2017.*

Wang, B. (2017). “Behaviour of pile foundations subjected to thermal loading.” Master of Engineering Thesis, Department of Civil Engineering, Monash University, Melbourne, Australia.

Wang, B., Bouazza, A., Singh, R., Haberfield, C., Barry-Macaulay, D. and Baycan, S. (2015). “Posttemperature effects on shaft capacity of a full-scale geothermal energy pile.” *Journal of Geotechnical and Geoenvironmental Engineering*, 141 (4), 10.1061/(ASCE)GT.1943-5606.0001266, 04014125-1-12.

Yavari, N., Tang, A. M., Pereira, J.M., and Hassen, G. (2016). “Effect of temperature on the shear strength of soils and the soil–structure interface.” *Canadian Geotechnical Journal*, 53(7), 1186-1194.

You, S., Cheng, X., Guo, H., and Yao, Z. (2016). "Experimental study on structural response of CFG energy piles." *Applied Thermal Engineering*, 96 (2016), 640-651.

Yu, K. L., Singh, R. M., Bouazza, A. and Bui, H. H. (2015). “Determining soil thermal conductivity through numerical simulation of a heating test on a heat exchanger pile.” *Geotechnical and Geological Engineering*, 33(2), 239-252.

Zhou, H., Kong, G., Liu, H., Wu, Y. and Li, G. (2016). “A novel cavity expansion-based analytical tool and its potential application for energy pile foundation.” *Energy Geotechnics: Proceedings of the 1st International Conference on Energy Geotechnics, ICEGT 2016, Kiel, Germany,* Wuttke A, Bauer S, and Sánchez, M, eds., CRC Press, London, UK, 359-365.

Table 1. Summary of ground conditions at the test site.

Depth (m)	Soil type	Soil description	In-situ test values	Gravimetric water content (%)
0 – 0.4	Fill material	Crushed rock silt, sand, moist, medium dense	–	–
0.4 – 3.5	Sandy clay	Silt, sand (sand lenses) moist, stiff - very stiff	S: 90 – 140 kPa SPT: 12 - 27	13 – 24
3.5 – 12.5	Sand	Sand, clay lenses, silt, cemented lenses, moist, dense	SPT: 25 – 30	5 – 13

S: Vane shear strength.

SPT N: Standard penetration test blow count.

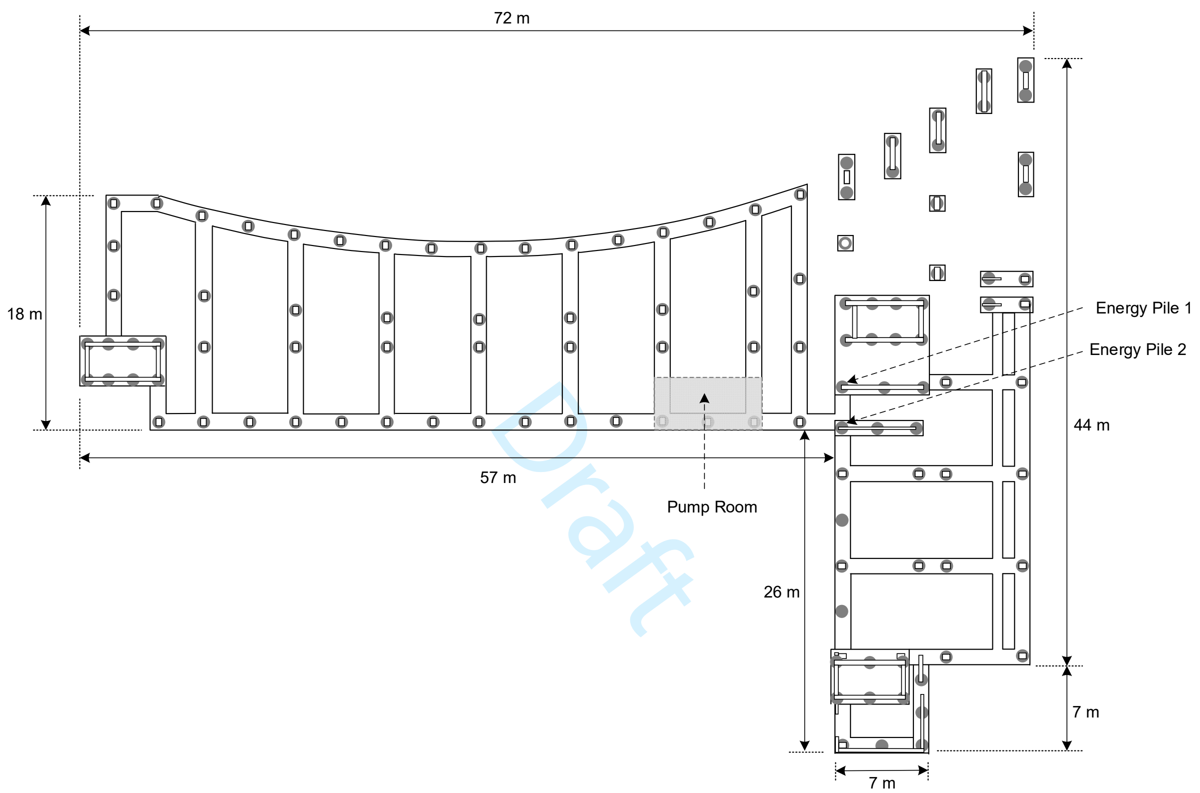

Fig. 1. Schematic of the pile layout of the building showing the locations of the energy piles and the pump room.

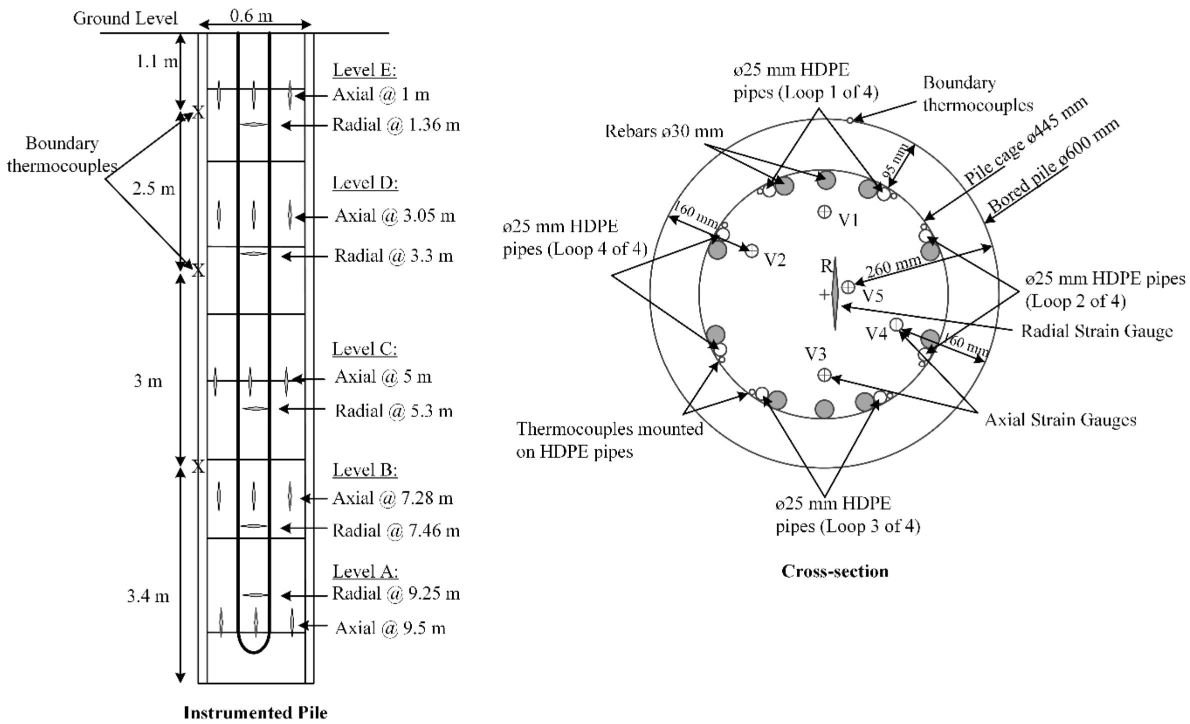

Fig.2. Schematic of the instrumented energy pile and a typical cross section showing the location of sensors at each depth.

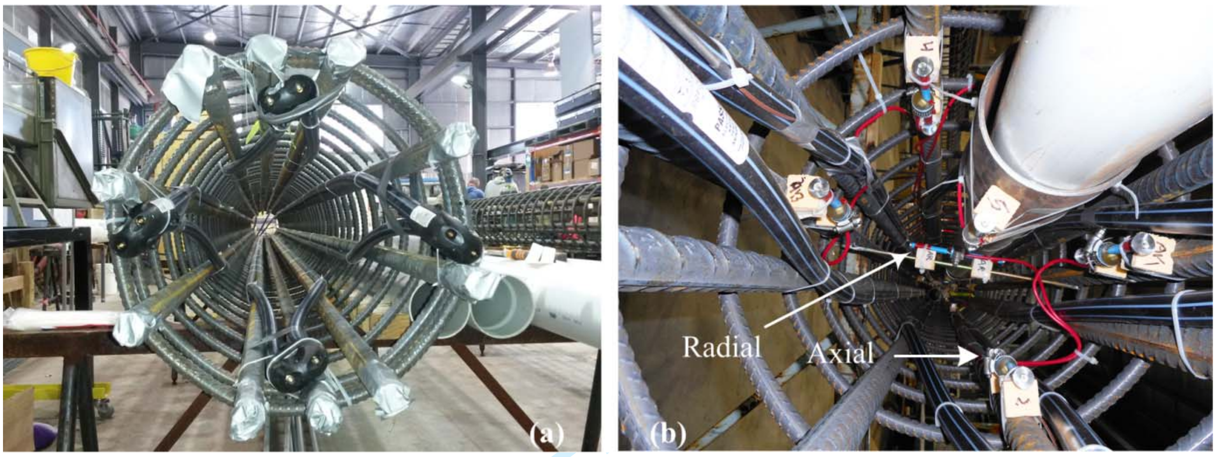

Fig. 3. Pile setup: a) U-loops inside the energy pile cage, b) axial and radial VWSGs inside the energy pile cage at a depth of 9.5 m.

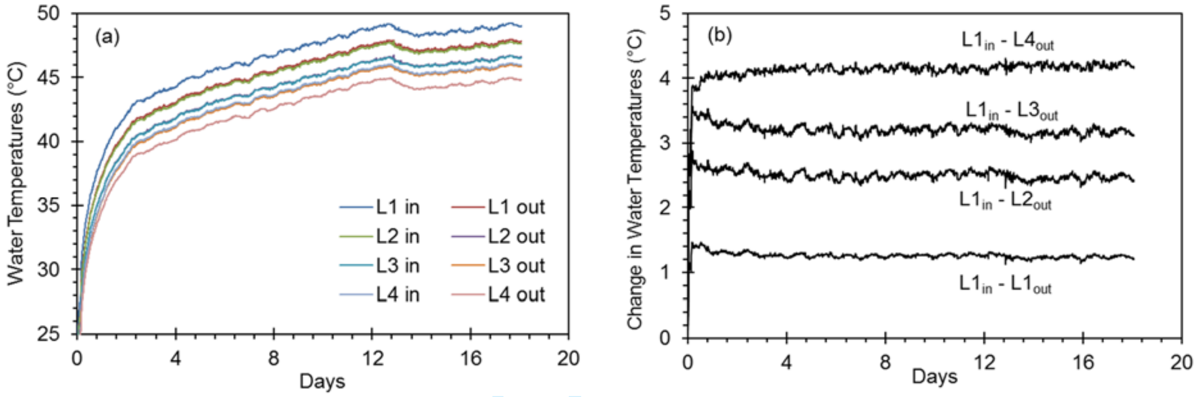

Fig. 4. Water temperatures (L: loop): a) water temperatures at the inlet and exit of each U-loop, b) change in water temperatures between the inlet of U-loop one and the exit of each U-loop.

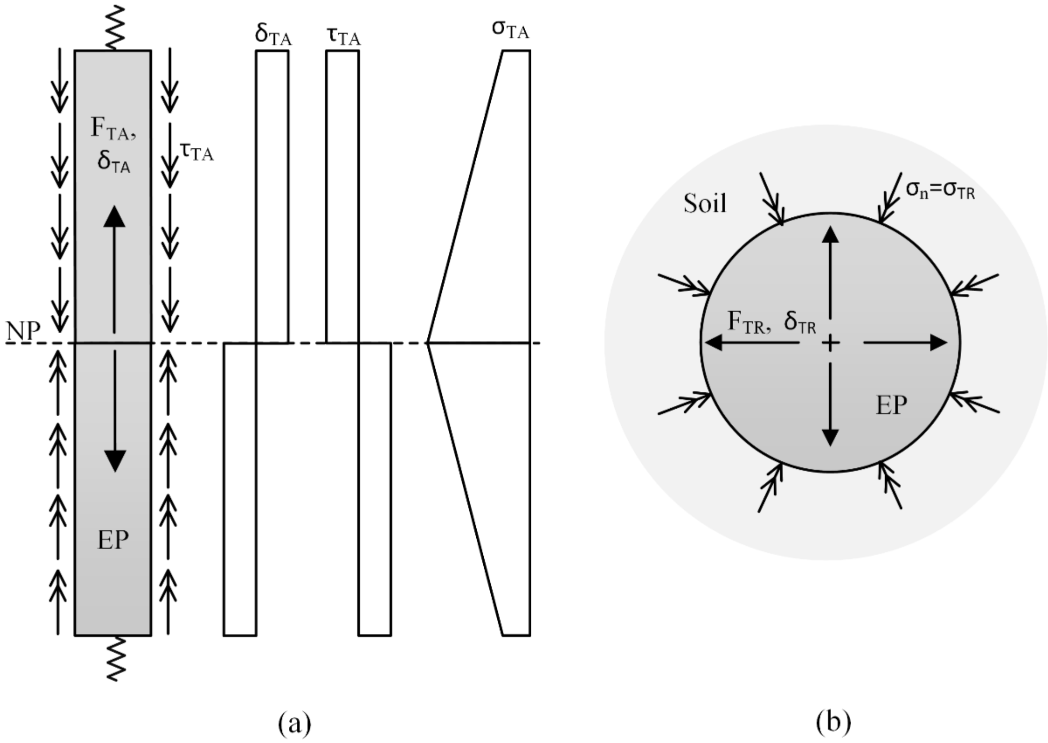

Fig. 5. Schematic of the thermal response of an energy pile with side and end restraints during heating (NP: null point, EP: energy pile, F_T: thermal force, δ_T: thermal displacement, τ_{TA}: thermally induced side shear stress, σ_T: thermal stress, σ_n: thermally induced normal stress, A: axial, R: radial): a) axial thermal response, b) radial thermal response.

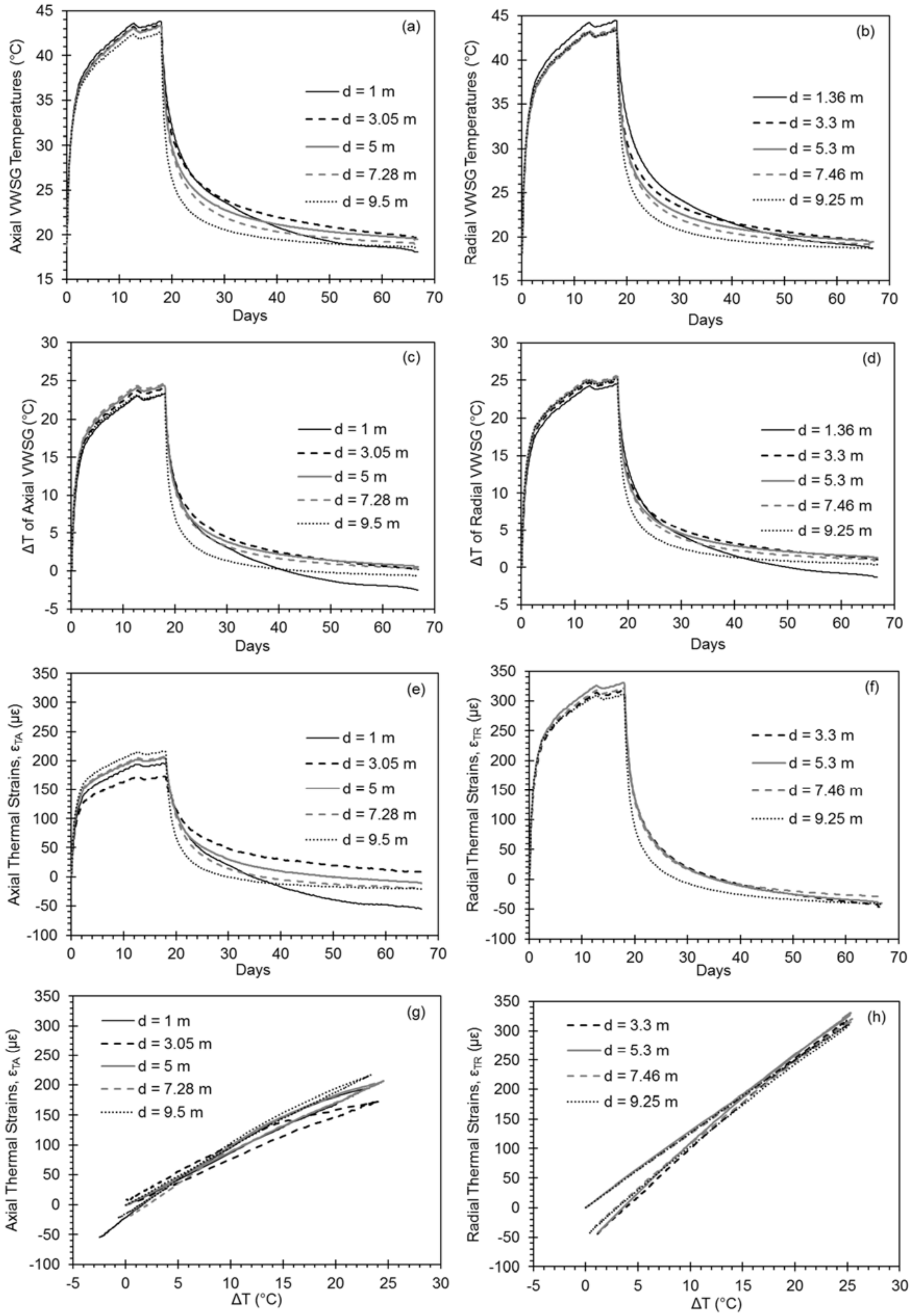

Fig. 6. Time series of pile temperatures and thermal strains: a) pile temperatures from axial VWSGs, b) pile temperatures from radial VWSGs, c) change in pile temperatures, *ΔT*, from axial VWSGs, d) change in pile temperatures, *ΔT*, from radial VWSGs, e) axial thermal strains, f) radial thermal strains, g) axial thermal strains plotted against change in pile temperature, h) radial thermal strains plotted against change in pile temperature.

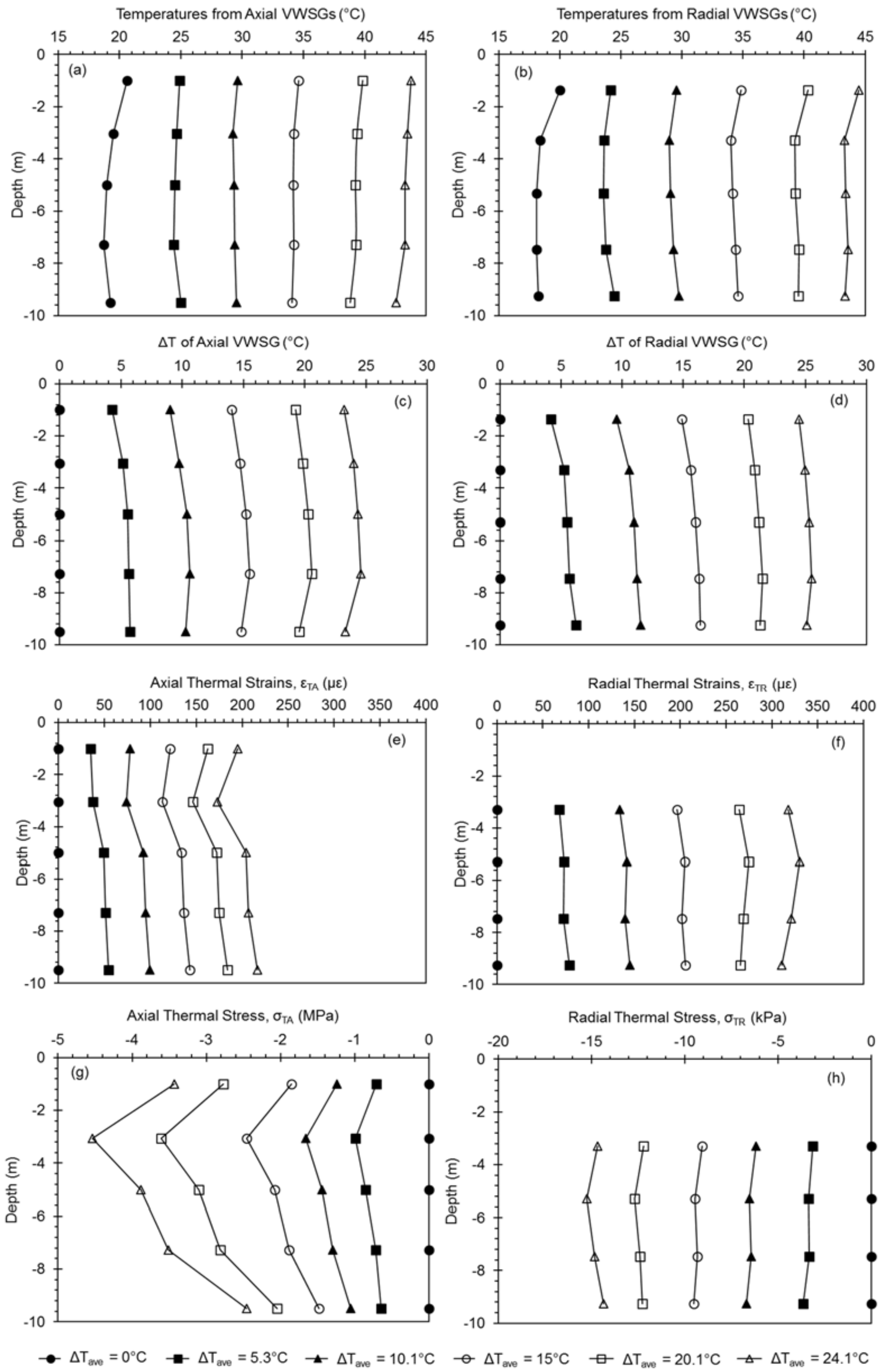

Fig. 7. Thermal responses against depth for different average changes in pile temperatures: a) pile temperatures from axial VWSGs, b) pile temperatures from radial VWSGs, c) change in pile temperatures, *ΔT*, of axial VWSGs, d) change in pile temperatures, *ΔT*, of radial VWSGs, e) axial thermal strains, f) radial thermal strains, g) axial thermal stresses, h) radial thermal stresses.

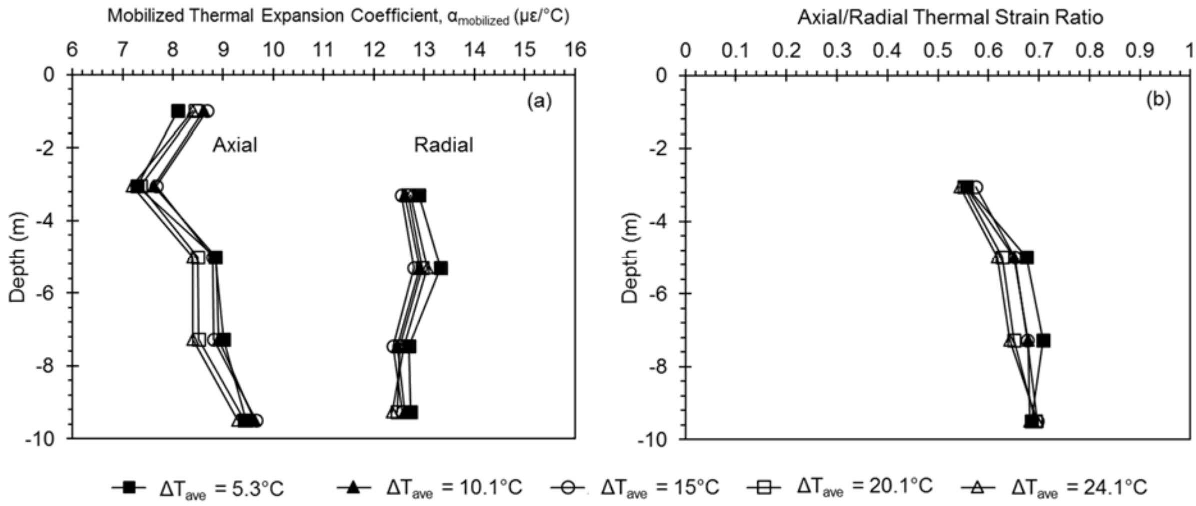

Fig. 8. Evaluation of thermal expansion: a) mobilized thermal expansion coefficients, b) ratio of axial and radial thermal strains.

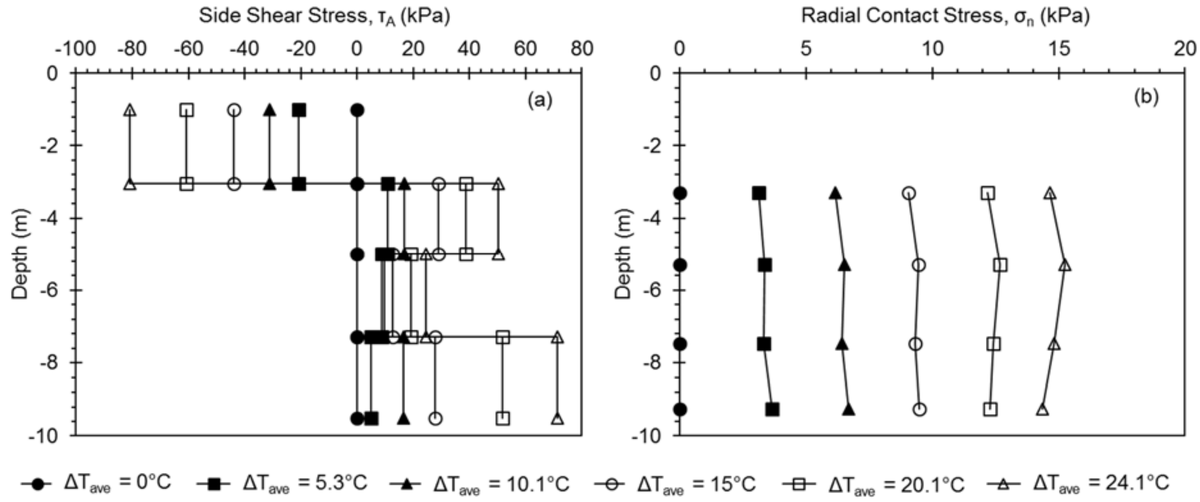

Fig. 9. Pile-soil contact stresses: a) side shear stresses mobilized by the axial thermal expansion of the pile, b) radial contact stresses mobilized by the radial expansion of the pile.

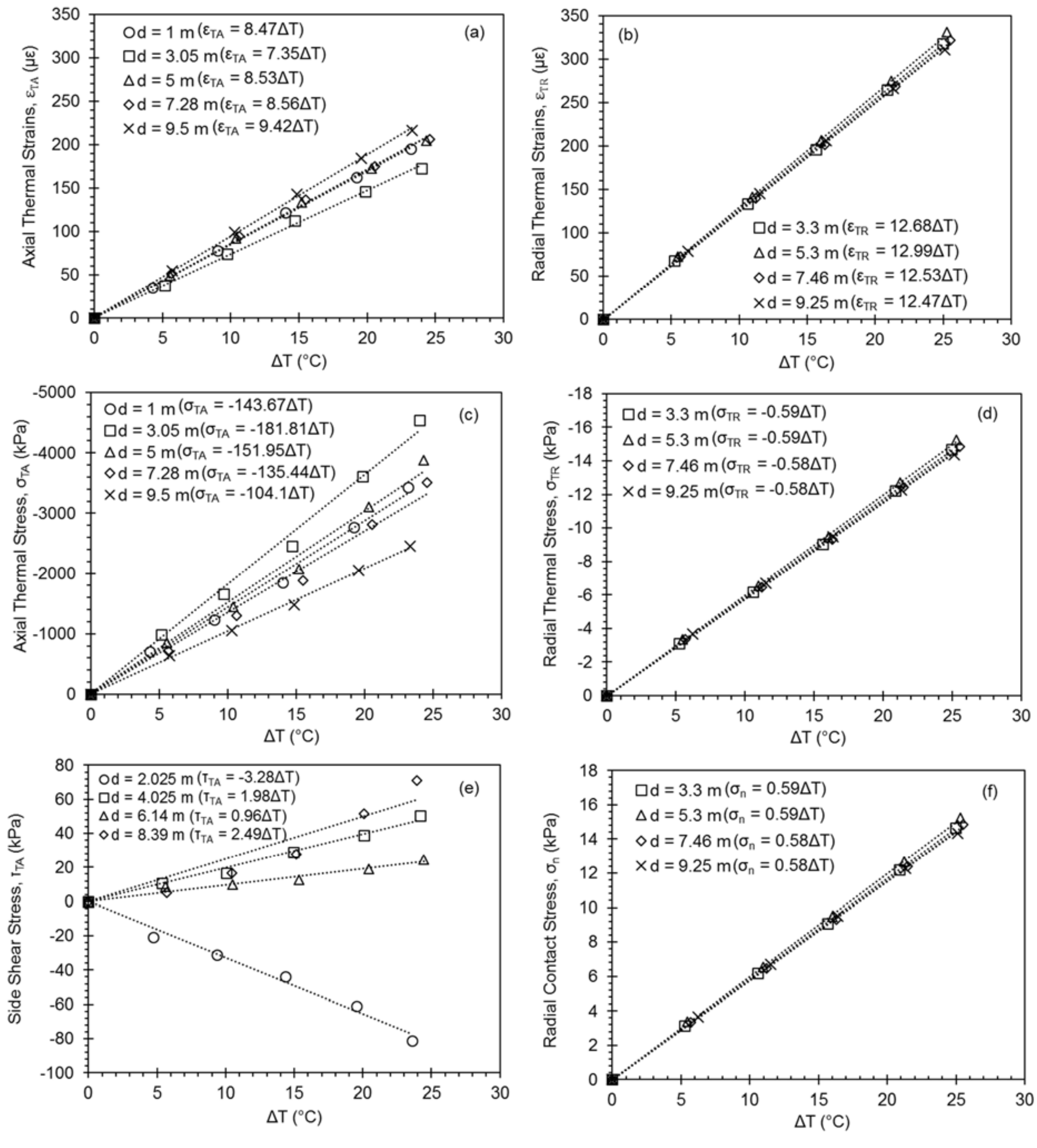

Fig. 10. Thermal responses plotted against ΔT: a) axial thermal strains, b) radial thermal strains, c) axial thermal stresses, d) radial thermal stresses, e) side shear stresses, f) radial contact stresses.

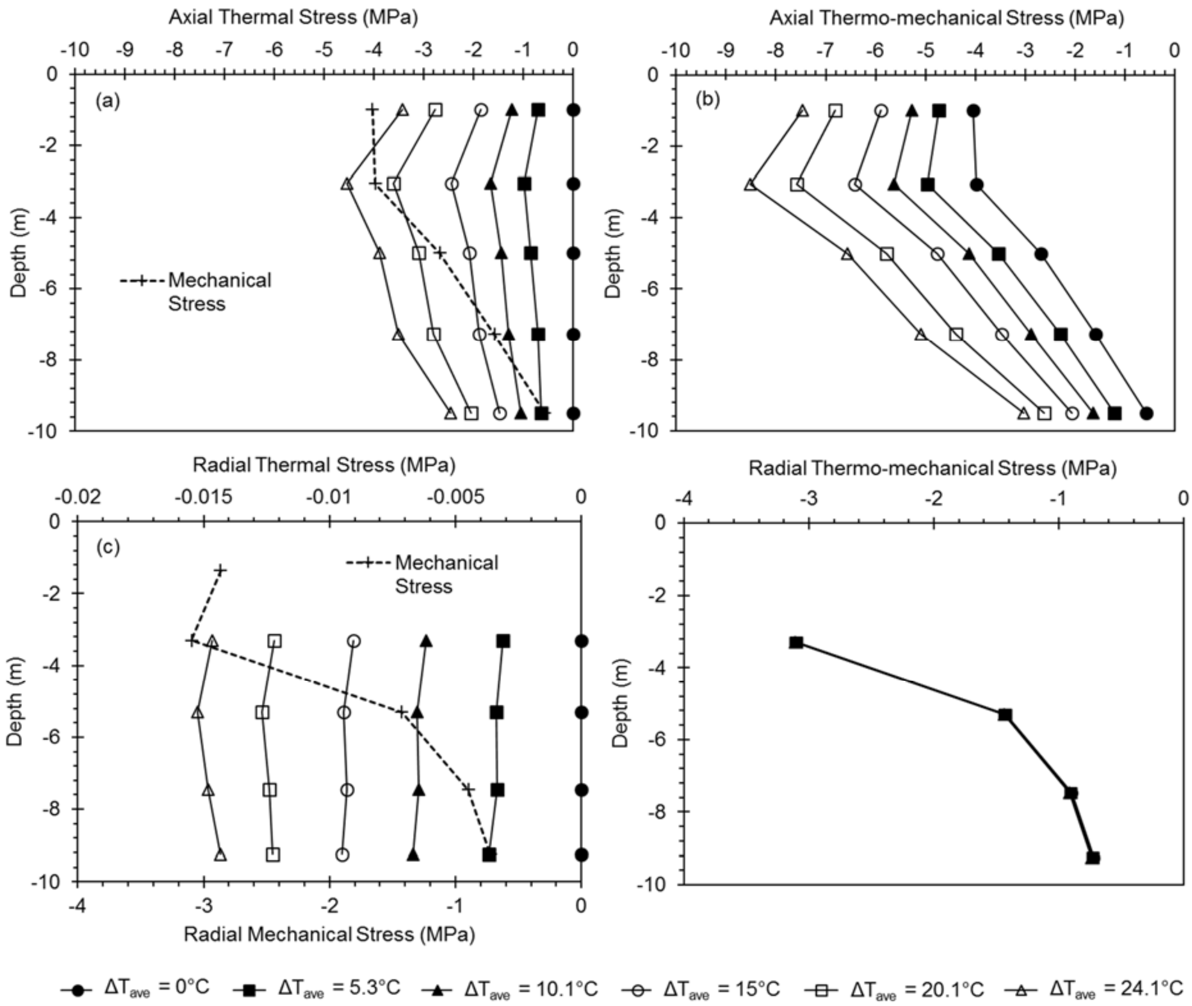

Fig. 11. Thermal and thermo-mechanical stresses: a) axial thermal stresses, b) axial thermo-mechanical stresses, c) radial thermal stresses, d) radial thermo-mechanical stresses.

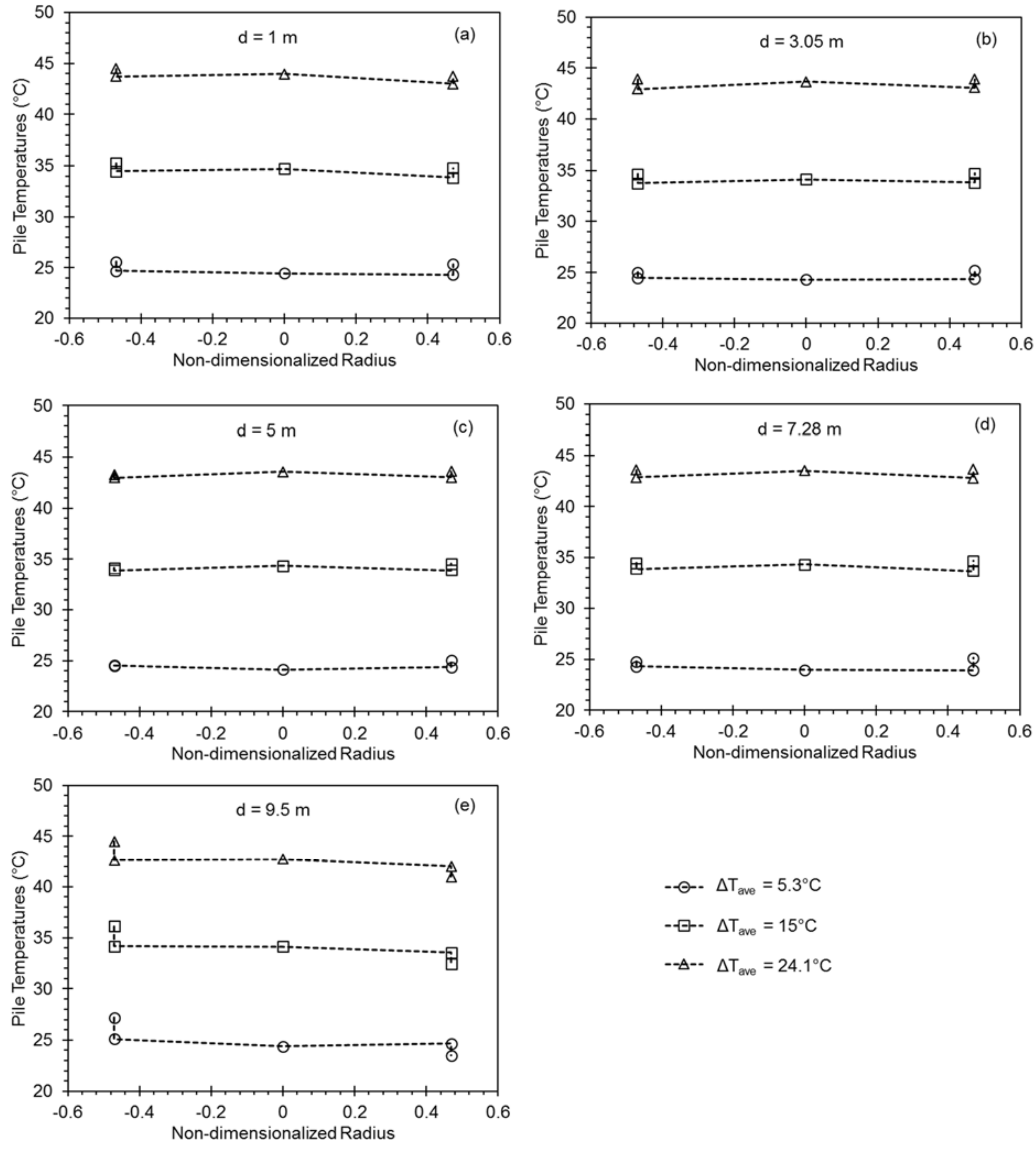

Fig. 12. Temperature distribution over the planar cross-section of the pile at different depths, *d*: a) d = 1 m, b) d = 3.05 m, c) d = 5 m, d) d = 7.28 m, e) d = 9.5 m.

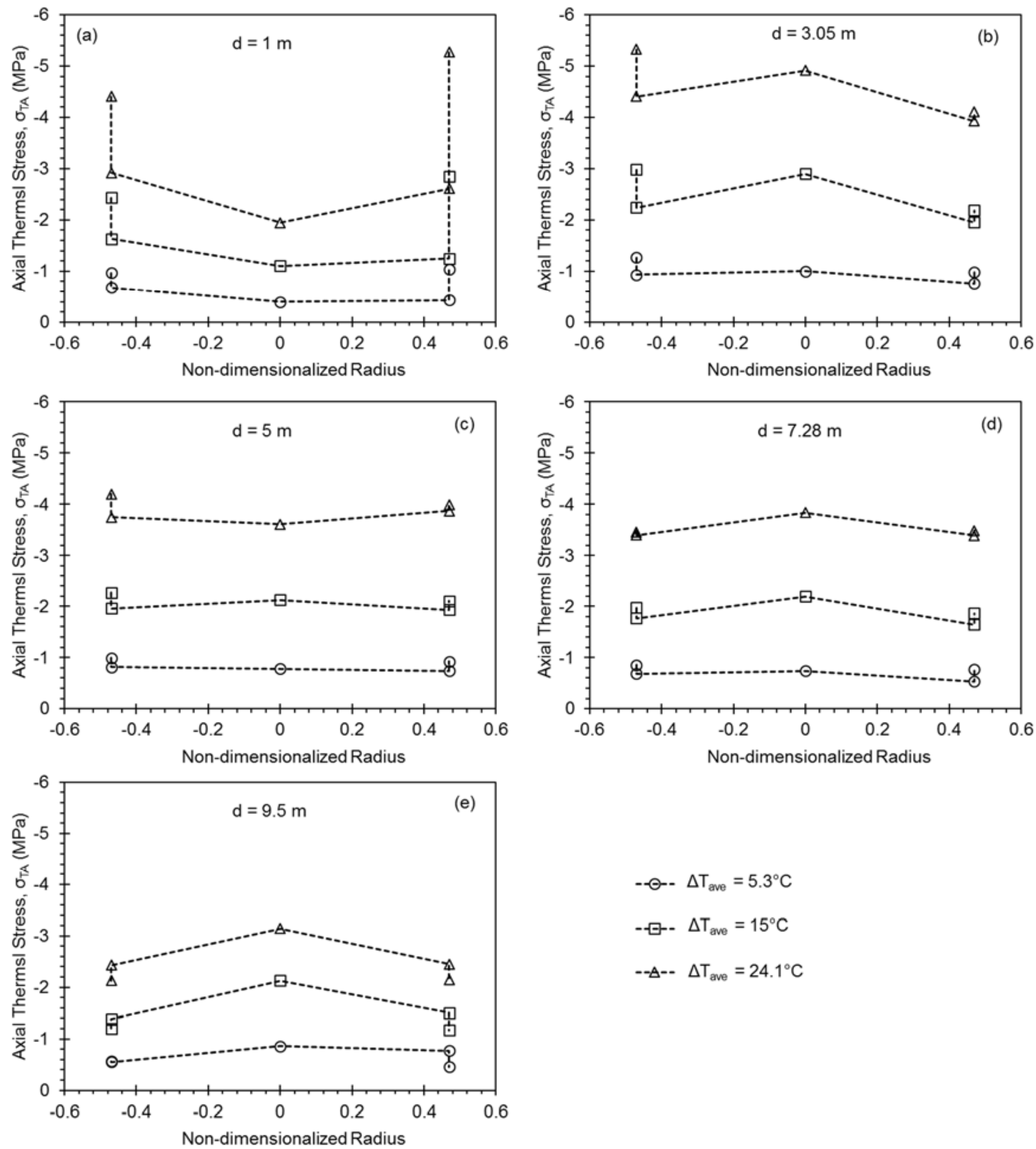

Fig. 13. Axial thermal stress distribution over the planar cross-section of the pile at different depths, *d*: a) d = 1 m, b) d = 3.05 m, c) d = 5 m, d) d = 7.28 m, e) d = 9.5 m.